1957BAN....14....1V

BULLETIN OF THE ASTRONOMICAL INSTITUTES OF THE NETHERLANDS

1957 NOVEMBER 9 VOLUME XIV NUMBER 480

COMMUNICATIONS FROM THE NETHERLANDS FOUNDATION FOR RADIO ASTRONOMY AND THE OBSERVATORY AT LEIDEN

ROTATION AND DENSITY DISTRIBUTION OF THE ANDROMEDA NEBULA DERIVED FROM OBSERVATIONS OF THE 21-cm LINE

BY H. C. VAN DE HULST, E. RAIMOND AND H. VAN WOERDEN

The atomic hydrogen emission from the Andromeda nebula (M31) was observed with the 25-metre telescope at Dwingeloo; the beamwidth was 0°.6. Line profiles were measured at 20 points of the major axis (Figure 5). The mean error of the brightness temperature measured at one frequency in one direction was 0.2 to 0.3°K except in the frequency range contaminated by galactic foreground radiation. The line was observable to 2°.5 at either side of the centre. The central velocity with respect to the local standard of rest is − 296 km/sec. The velocity of rotation slowly falls from 278 km/sec at 0°.6 from the centre to 221 km/sec at 2°.5 (Table 7). The accuracy is well within 10 km/sec. The density distributions determined from the integrated profiles in the SW and NE halves of the system separately show pronounced peaks at 1° from the centre in each half (Table 6). Model line profiles were computed with the average density distribution of the two halves on the assumption of circular symmetry, taking full account of the antenna pattern. They fit the observed profiles quite well if a broadening effect is introduced corresponding to random cloud motions with a root mean square velocity of 8 km/sec. The total mass of atomic hydrogen in the system is $0.25 \times 10^{10}\ c^2$ solar masses if the distance of M31 is 500 c kpc; it is 0.01 c times the total mass of M31 determined by SCHMIDT in the succeeding paper. Both the hydrogen mass and the total mass exceed those of the Galactic System. A local excess of radiation found at $v = -224$ km/sec in the NE part of the system has been investigated by more complete measurements but no satisfactory explanation has been found.

1. *Observations*

Among the very first programmes of the 25-metre radio telescope at Dwingeloo (VAN DE HULST, HOOGHOUDT, SCHOR, HUISMAN, SCHIERBEEK, JÖBSIS, 1957) was an investigation of the 21-cm hydrogen radiation from the Andromeda Nebula (M31). The observations reported here were made from October 12 to November 5, 1956, and January 3 to 27, 1957. The total observing time was about 320 hours. The altitude at each observation was $> 23°$.

In the preceding period the telescope had been equipped with a receiver for measuring the continuous radiation near 21 cm and a dipole-disk feed at the focus. The disk was somewhat bent toward the dipole in the H-plane in order to make the antenna pattern in the E- and H-planes equally wide. Table 1, kindly supplied to us by Mr WESTERHOUT, gives the pattern for this feed, based on measurements of the Cas A source and corrected for the non-linear detector law (see Figure 1).

Observing the 21-cm line with a reasonably flat zero line over a wide frequency range necessitated bringing the mixer and first stage of i.f. amplification to the focus. They were mounted in a cubic box with sides of 20 cm, attached behind the disk of a new dipole-disk feed, carefully dimensioned after the first one. The antenna pattern of this feed determined at the frequency of the deepest absorption line in the Cas A spectrum (MULLER, 1957) matched the pattern given in Table 1. We assume that the pattern

TABLE 1

Antenna pattern

r	$p(r)$
°	
0.0	1.00
0.1	0.92
0.2	0.71
0.3	0.45
0.4	0.24
0.5	0.10
0.6	0.02
0.7	0.00

CONTENTS

© Astronomical Institutes of The Netherlands • Provided by the NASA Astrophysics Data System

1957BAN....14....1V

FIGURE 1

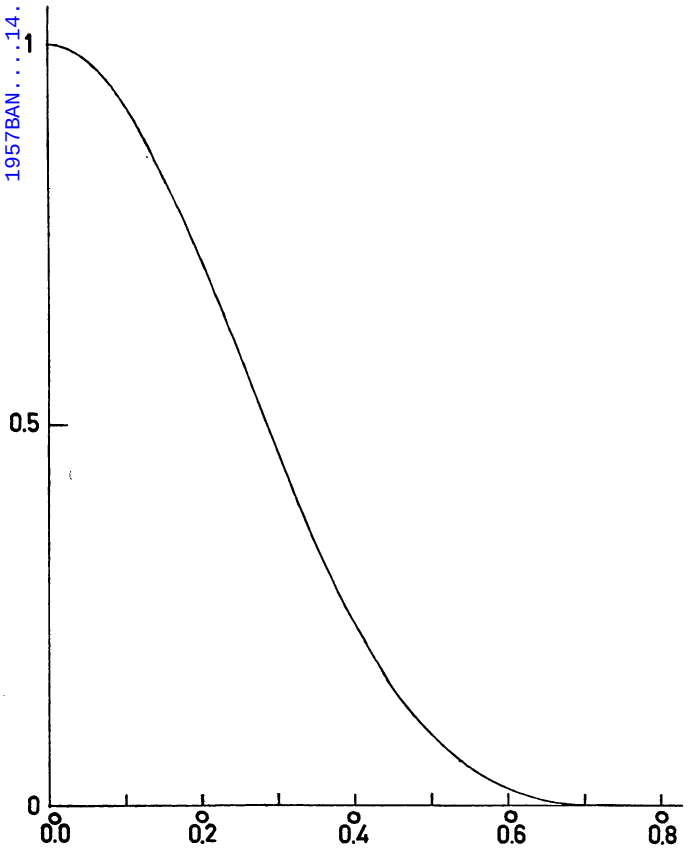

Antenna pattern.

is circularly symmetric. The width between half-power points is 0°.57. Any undetected side lobes, which are certainly below 1 per cent (20 db), are irrelevant in this investigation.

The telescope was equipped with a new 21-cm line receiver, designed and built by Mr MULLER as a general-purpose instrument that can be used with different bandwidths over a wide frequency interval. The normal mode of operation gives an automatic comparison with two equally wide channels 1.08 Mc/s at either side of the measuring channel. One or the other or both comparison channels may be used. The last stage of the first local oscillator was behind the vertex of the paraboloid. The further receiver was in the observing house below the mirror. This new receiver is an improved version of the one described by MULLER and WESTERHOUT (1957).

A large bandwidth was chosen for this investigation. The width was 135 kc/s between half-power points and 150 kc/s if defined as the ratio of the integral to the maximum. The first observations were made with the automatic frequency scan in operation in order to record directly a line profile but the profile could not clearly be distinguished from zero drifts. Scans through the nebula at a fixed frequency gave more definite results with maximum intensities of the order of 5°K, i.e., somewhat less than expected on

FIGURE 2

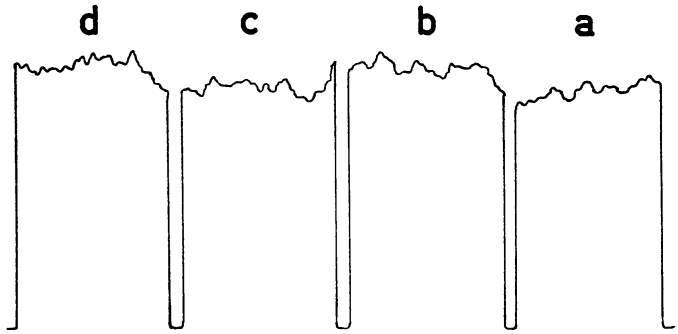

Sample record of one hour's observation, $\Delta T = 1.3$°K.

the basis of a prognosis (VAN DE HULST, 1957).

In order to improve the accuracy by which such small intensities may be measured, a different method was adopted throughout the observing period. The normal mode of operation was as follows. The frequency was kept constant during one hour, during which we set 15 minutes on a selected point in the nebula, 15 minutes on a comparison field, again 15 minutes on the measuring point, and again 15 minutes on the comparison field. The time constant was 54 sec. Figure 2 shows a typical record. The average readings during each 15 minute interval were obtained by eye estimate, discarding the first few minutes. If the readings are denoted by a, b, c, d, the systematic difference was computed as the average of

$$\tfrac{1}{2}(a + c) - b \text{ and } c - \tfrac{1}{2}(b + d). \qquad (1)$$

This method allows for a uniform drift during the hour; the result is identical to the solution by the method of least squares. The fixed comparison field used at most frequencies was 4° from the centre of the nebula and may be assumed to have no hydrogen emission except in the frequency band corresponding to velocities between + 40 and − 110 km/sec with respect to the local standard of rest. Hence the difference obtained is the intensity at one point in a line profile.

Other points of the profile are obtained by repeating the process for other velocities. Often, a full profile could just be completed in one night.

Variations on this method were necessitated by the possible appearance of hydrogen-line radiation from M31 in the comparison channels or hydrogen-line radiation from the Galactic System in the measuring or comparison channels. The majority of the complications that might have arisen from these effects were avoided by not using the disturbed comparison channel. If the left (or right) comparison channel has been used and was assumed to be free of any line radiation, the left (or right) side of the circle in Figure 5 has been filled in. If the left (or right) comparison channel has not been used, this side of the circle has been left blank.

© Astronomical Institutes of The Netherlands • Provided by the NASA Astrophysics Data System

1957BAN....14....1V

Complications were unavoidable in the following situations.

Radiation from M31 in a comparison channel. This situation occurred when the other channel had to be avoided for fear of galactic line radiation. It also occurred in the profiles near the centre of the nebula, because the extent of the wings of the line profiles was underestimated initially. The normal remedy was to make a measurement at the frequency of the disturbed comparison channel (this always made the new comparison channel free) and to add the result to the earlier one. A few measurements with galactic radiation in a comparison channel were corrected in the same manner. A measurement which has been corrected in this manner for line radiation in the left (or right) comparison band has been indicated by a shaded left (or right) half of the circle in Figure 5. In a few instances an estimated correction was used.

Galactic hydrogen line radiation in the measuring band. As the centre of M31 approaches us with a velocity of the same order as the rotational velocity in its outer parts, the gas at one side of M31, the NE side, is almost at rest with respect to the sun. Consequently, the galactic foreground radiation has to be eliminated. The only method of separation, in principle, is to make at each frequency an isophote map of M31 and the surrounding area. If the surrounding region is sufficiently smooth, the galactic radiation at a point within the contours of M31 may be estimated by interpolation.

As a shorter version, any point suspected of galactic radiation in the measuring band was measured with two comparison fields. These fields were chosen symmetrically at both sides of the measured field. Each measurement lasted 6×15 minutes, in the order $a\ b\ c\ d\ e\ f$, with a,d = first comparison field, b,e = measured field, c,f = second comparison field. The resulting value of the M31 emission was computed as the average of

$$\begin{array}{lll} b - (\frac{2}{3}a + \frac{1}{3}d) & , & (\frac{2}{3}b + \frac{1}{3}e) - c \\ (\frac{1}{3}b + \frac{2}{3}e) - d & , & e - (\frac{1}{3}c + \frac{2}{3}f). \end{array} \qquad (2)$$

Points in Figure 5 which have been obtained by this method are drawn as squares. Open, shaded, or filled-in halves of the squares have the same meaning as those of the circles, explained above.

The measured fields were centred at points on the major axis at a distance $x \times 0°.25$ from the centre. The centre of the nebula is at $\alpha = 10°.092$, $\delta = 41°.037$ (1956.9) and the position angle of the major axis is 38°. The positions of the comparison fields are shown in Figure 3. The standard comparison field (A) is at $\alpha = 15°.00$, $\delta = 41°.00$. The far sequence of comparison fields is diametrically opposite to A with respect to the points on the NE end of the major axis (negative x). Later, a number of points were measured with nearby comparison fields. The near sequences are just far enough from the nebula to be sufficiently clear of radiation from M31.

FIGURE 3

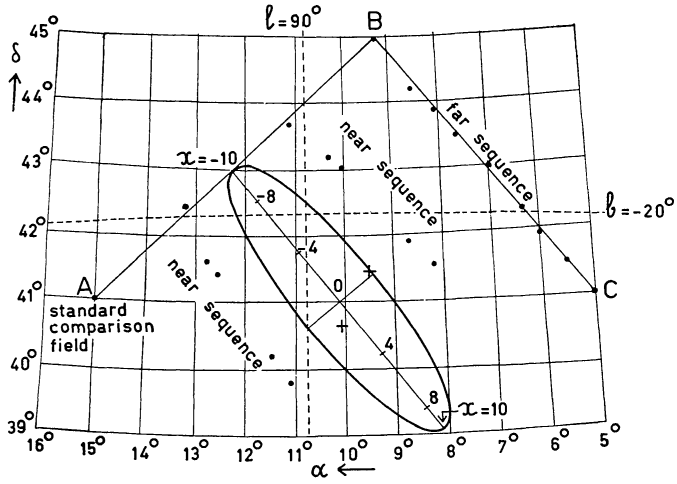

Sketch of nebula and comparison fields (indicated by dots). Positions of M32 and NGC 205 are shown by plus signs.

2. *Corrections and estimated errors*

The frequencies were set with an accuracy better than 10 kc/s and were reduced to velocities with respect to the local standard of rest using the tables of MACRAE and WESTERHOUT (1956).

The positions were computed and set on the α and δ scales of the telescope with an accuracy of 0°.01. The telescope amply meets the design figure of an error $< 0°.05$; under favourable circumstances, the positioning error is smaller than 0°.03. However, the measurements usually were not interrupted when a strong wind caused a difference of the order of 0°.05 between the positions of the pilot (automatic coordinate converter) and the telescope. Considering all causes of deviation, errors of 0°.02 in position are probable, 0°.05 exceptional, and 0°.10 very exceptional in this programme. Refraction corrections, which would have amounted to 0°.04 at the most, were omitted.

The unit of intensity in this paper will be called a degree Kelvin, although an absolute determination was not attempted. The precise definition is that 70 units = intensity of top of profile at $l = 50°$, $b = 0°$, with the 150 kc/s bandwidth. The top intensity of the same profile recorded with the 40 kc/s bandwidth is 96, which agrees sufficiently well with the value of 100 units on the scale used in *B.A.N.* No. 452 (VAN DE HULST, MULLER and OORT, 1954) and *B.A.N.* No. 475 (MULLER and WESTERHOUT, 1957).

Variations of the intensity scale were determined and corrected as follows.

a) Differences of sensitivity between the receiver

© Astronomical Institutes of The Netherlands • Provided by the NASA Astrophysics Data System

1957BAN..14..1V

used with comparison channel 1, or 2, or both combined, cannot occur, because of the automatic gain control, unless something is drastically misadjusted. Tests showed no differences within a few per cent. No corrections were applied.

b) The sensitivity gradually decreased with time, because of a gradual increase of the noise figure. An accurate check on this variation was afforded by daily measurements of the top of the line profile at $l = 50°$, $b = 0°$. The corrections applied for this effect range from -1 to $+1$% in October-November and from -5 to $+2$% in the January observing period.

c) The sensitivity shows a systematic variation with frequency because, for technical reasons, the central frequency of the 30 Mc/s i.f. amplifier does not coincide with the frequency of minimum noise figure. This effect was measured. The corrections to be applied were found by interpolation from Table 2.

TABLE 2

f(Mc/s)	v'(km/sec)	corr.	f(Mc/s)	v'(km/sec)	corr.
34.0	+ 479	− 1.5%	37.0	− 154	+ 1%
34.5	+ 373	− 1	37.5	− 260	3
35.0	+ 268	− 1	38.0	− 365	5.5
35.5	+ 162	− 1	38.5	− 471	9
36.0	+ 57	− 0.5	39.0	− 576	13
36.5	− 49	0	39.5	− 682	19

Here f is the frequency of the second local oscillator and v' is the hydrogen velocity in the line of sight, not corrected for the motions of the Sun and Earth.

d) Extinction was neglected as it remained < 2%.

The points plotted in Figure 5 represent the intensity values obtained after these corrections have been applied. They form the basis of the theoretical discussion in the following sections. The numerical data are given in the table opposite the Figure.

With measurements so near the limits of what is feasible, it is very hard to be certain that systematic errors are avoided. Only a few observations could be repeated in the available time. Some unexplained differences were found. For instance, the points at $x = 3$, $v = -522$ km/sec, $T = 4.2$°K, and at $x = 2$, $v = -385$ km/sec, $T = 2.4$°K, measured on the same day in January, are both about 20 per cent lower than the curve through the other measurements, which were made in October. Other similar checks gave better agreement. On the whole, the data in Figure 5 appear quite consistent.

The accuracy of the ordinates of the points in Figure 5 is limited by four effects, which will be discussed separately.

A. Sensitivity changes.

B. Position errors.

C. The limited time over which the noise is averaged.

D. (For the squares) Errors of interpolation in the assumed galactic radiation.

A. The calibration readings on $l = 50°$, $b = 0°$ show day-to-day random variations with a root mean square value of $2\frac{1}{2}$ per cent from the linear decrease for which a correction was applied. These sensitivity variations hardly affect the points in Figure 5.

B. The temperature error which may be caused by an error of 0°.05 in position may be estimated from Figure 5 as one fifth of the temperature difference between adjacent profiles at the same velocity. Such errors may have introduced intensity errors of the order of 0.4°K here and there; errors of 0.2°K may have been fairly common.

C. Let the reading obtained by averaging the recorded intensity with two comparison channels at a fixed frequency at a fixed point of the sky during $t = 12$ minutes have a mean error μ. The average temperature value from (1) then has the mean error $\mu\sqrt{\frac{5}{4}}$ if two free comparison channels have been used (symbol ●). On the other hand, the difference of the two values in (1), namely

$$\tfrac{1}{2}(a - b - c + d) \qquad (3)$$

has exactly the mean error μ. For measurements with one free comparison channel and the other channel not used (symbol ◑ or ◐), the mean error of the derived temperature is $\mu\sqrt{\frac{5}{2}}$ and of the difference, $\mu\sqrt{2}$. Similarly the temperature values marked by the symbols ◍, ⊕ and ⊖ have calculated mean errors $\mu\sqrt{\frac{15}{4}}$, $\frac{5}{2}\mu$ and $\mu\sqrt{5}$, respectively.

The value of μ was determined from the statistics of the differences (3) in three homogeneous groups as shown in the following table.

	number of points	rms difference	μ
October, 2 free channels	66	0.18	0.18
October, 1 free channel	32	0.24	0.17
January, 1 free channel	23	0.19	0.14

These empirical values of μ are in good agreement with the theoretical value (MULLER, 1956),

$$\Delta T = 1.03\frac{\pi}{\sqrt{2}}(N - 1)\, T_\circ\, (F.\Delta\nu.\tau)^{-\frac{1}{2}}, \qquad (4)$$

which by substitution of $N = 3$, $T_\circ = 293°$, $F = 1.53$, $\Delta\nu = 150$ kc/s, $\tau = 360$ sec [1]), gives

$$\Delta T = 0.15°\text{K}.$$

[1]) It may be shown that in taking the straight average of the recorded intensity during a time t, the appropriate time constant in this formula is $\tau = {}^1/_2\, t$; see, for instance, MANN and MEZGER (1956).

© Astronomical Institutes of The Netherlands • Provided by the NASA Astrophysics Data System

1957BAN....14....1V

The empirical values include the errors made in estimating the average deflection for the 12 minutes record and those arising from inaccurate guiding and from variations in receiver drift during the hour. These errors seem to have had little effect.

Taking $\mu = 0.16°K$ as a representative average, we find that the mean errors of the points indicated in Figure 5 by different circle symbols range from 1.12 $\mu = 0.18°K$ to 2.5 $\mu = 0.40°K$. The mean error of an average point in Figure 5 remains well below 0.3°K.

D. The accuracy of the points indicated by squares would be better because longer time has been spent on each. If two free comparison channels have been used (symbol ■), the average value of the expressions (2) is found to have the mean error

$$\mu\sqrt{\tfrac{7}{9}} = 0.14°K.$$

However, this advantage is offset by the error made in assuming that the galactic foreground in the measured field is exactly the average of that in the two comparison fields.

FIGURE 4

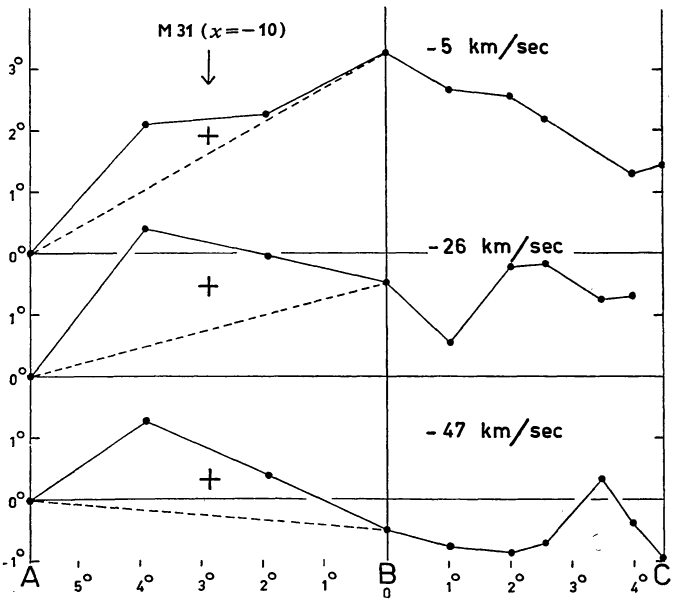

Galactic foreground radiation along track ABC at three frequencies.

These errors are serious in the range $v = -70$ to 0 km/sec. An impression of their order of magnitude is given by Figure 4, which shows the measured intensity relative to point A along the track ABC in Figure 3. The points between B and C in the two lower curves have a measured mean deviation 0.45°K from the average, i.e., a true mean deviation $h = 0.41°K$. The error made in taking from a set of values with this mean deviation the average of two arbitrary points (the comparison fields) instead of a third one wanted (the measured field) is $h\sqrt{\tfrac{3}{2}} = 0.50°K$. When combined with the measuring error this becomes 0.52. The fact that the average of the near comparison fields differs by more than 1°K from the average of the far comparison fields, suggests a mean error of a similar magnitude. The crosses in Figure 4 indicate the value adopted for galactic radiation at the field of the nebula.

The combined uncertainty of the uneven foreground and the measuring error gives the following estimated mean errors (Table 3) of the filled squares in Figure 5, as a function of the velocity v with respect to the local standard of rest. The errors for the squares that are not fully filled are only slightly larger.

TABLE 3

v (km/sec)	mean error (°K)
+ 37	0.25
+ 16	0.30
− 5	0.45
− 26	0.55
− 47	0.55
− 69	0.35
− 90	0.25
− 111	0.20

3. *Radial velocity of the centre*

The radial velocity of the centre of gravity of M31 was determined from the data in Figure 5 by the following method [1]). The profiles in two points at equal distance from the centre are compared and all ordinates of one profile are multiplied by a common factor to give the profiles approximately equal height. This allows for asymmetries in the mass distribution. One profile is then drawn on transparent paper, is put with inverse velocity scale on the other one, and is shifted sideways until the best coincidence is found. The radial velocity of the centre, v_c, then is half the sum of coinciding velocities of the two profiles. The method was applied to 7 pairs of profiles and to the

TABLE 4

field x ($\frac{1}{4}°$)	T multiplied by NE	SW	$v_c \pm$ m.e. (km/sec)
0	—	—	− 297 ± 4
1	1	1.2	− 308 ± 4
2	1	1.25	− 307 ± 4
3	1	1	− 303 ± 2
6	1	1.1	− 291 ± 2
7	1.2	1	− 290 ± 2
8	1.5	1	− 290 ± 3
10	1	1	− 273 ± 20
Dwingeloo, weighted mean			− 296 ± 3
Mt Wilson / Lick (HUMASON, MAYALL and SANDAGE, 1956)			− 262 ± 20 / − 286 ± 30

[1]) We acknowledge the help of Miss L. M. J. S. VOLDERS in this part of the investigation.

© Astronomical Institutes of The Netherlands • Provided by the NASA Astrophysics Data System

1957BAN....14....1V

FIGURE 5

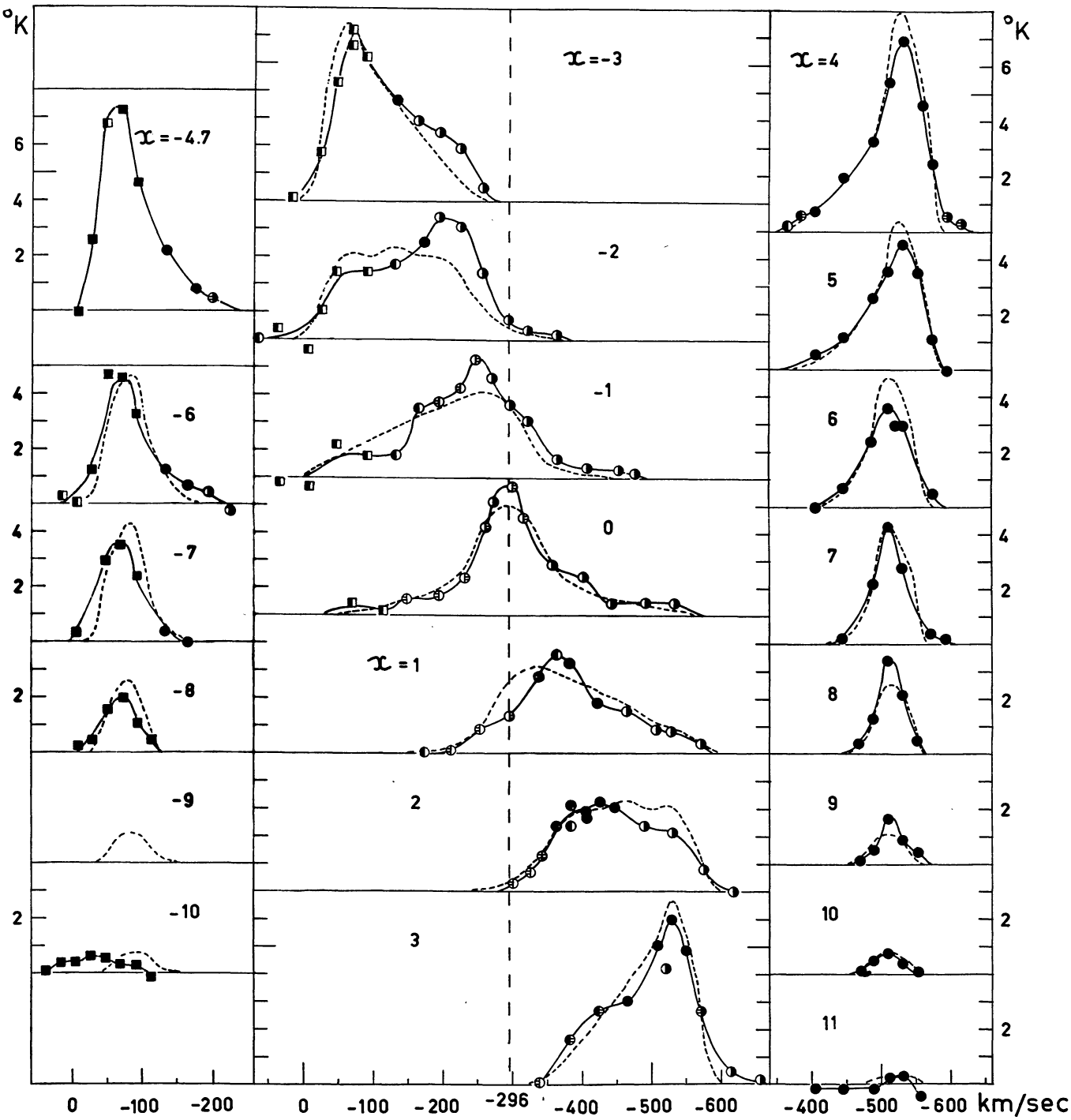

Line profiles in points on the major axis. Symbols of various kinds and solid curves: observations. Dotted curves: profiles computed for a model nebula.

profile at $x = 0$ by inverting the right half on the left half. The results are shown in Table 4.

The precision of the result may be found by trying out what changes in the sideways shift are allowable. These estimates were fully confirmed by a more formal computation of the mean error as follows.

Let η be the mean error of the ordinate, T, of a point of unit weight (a full circle in Figure 5) and let p be the weight of an arbitrary point. If a coincidence is obtained at a provisional value of the centre velocity, v_c', a smooth curve may be drawn through all points. Each point has a residual Δ' from this curve at a place where the slope of the curve is $s = \frac{dT}{dv}$.

A further shift of all points of profile 1 by the velocity correction u_1 changes the residuals to $\Delta = \Delta' + su_1$.

© Astronomical Institutes of The Netherlands • Provided by the NASA Astrophysics Data System

1957BAN....14....1V

Tabular data belonging to Figure 5

x and y, rectangular coordinates in $^1/_4°$; α and δ, coordinates as set on scales (1957.0); v in km/sec with respect to the local standard of rest, T in °K (see p. 3)

$x = -10$, $\alpha = 12°.16$, $\delta = 43°.01$

v	T
+ 37	0.1
+ 16	0.4
− 5	0.4
− 26	0.8
− 47	0.6
− 69	0.3
− 90	0.3
− 111	− 0.2

$x = -8$, $\alpha = 11°.76$, $\delta = 42°.61$

v	T
− 8	0.2
− 28	0.5
− 50	1.5
− 71	2.0
− 92	1.1
− 113	0.5

$x = -7$, $\alpha = 11°.54$, $\delta = 42°.42$

v	T
− 5	0.3
− 47	2.9
− 69	3.5
− 90	2.4
− 132	0.4
− 164	0.0

$x = -6$, $\alpha = 11°.33$, $\delta = 42°.22$

v	T
+ 16	0.3
− 5	0.0
− 26	1.2
− 47	4.7
− 69	4.6
− 90	3.3
− 132	1.2
− 164	0.7
− 195	0.4
− 225	− 0.2

$x = -4.7$, $y = -0.3$, $\alpha = 11°.12$, $\delta = 41°.92$

v	T
− 6	− 0.1
− 27	2.6
− 48	6.7
− 70	7.2
− 91	4.6
− 133	2.2
− 175	0.8
− 199	0.5

$x = -3$, $\alpha = 10°.71$, $\delta = 41°.63$

v	T
+ 16	0.1
− 26	1.8
− 47	4.3
− 69	6.2
− 69	5.6
− 90	5.2
− 132	3.6
− 164	2.9
− 195	2.5
− 225	1.9
− 258	0.5

$x = -2$, $\alpha = 10°.50$, $\delta = 41°.43$

v	T
+ 64	0.0
+ 37	0.4
− 5	− 0.4
− 26	1.0
− 47	2.5
− 90	2.4
− 132	2.7
− 174	3.5
− 195	4.4
− 225	4.0
− 258	2.4
− 294	0.7
− 322	0.4
− 364	0.2

$x = -1$, $\alpha = 10°.30$, $\delta = 41°.23$

v	T
+ 33	− 0.1
− 5	− 0.4
− 47	1.2
− 90	0.8
− 132	0.8
− 164	2.5
− 195	2.8
− 225	3.3
− 248	4.3
− 271	3.6
− 294	2.6
− 322	2.1
− 364	0.7
− 406	0.4
− 453	0.3
− 476	0.2

$x = 0$, $\alpha = 10°.09$, $\delta = 41°.04$

v	T
− 69	0.4
− 114	0.2
− 149	0.6
− 191	0.7
− 233	1.4
− 262	3.2
− 275	4.1
− 302	4.7
− 317	3.6
− 359	1.8
− 401	1.4
− 444	0.4
− 491	0.5
− 533	0.5

$x = 1$, $\alpha = 9°.89$, $\delta = 40°.84$

v	T
− 175	0.0
− 212	0.1
− 254	0.9
− 297	1.3
− 339	2.8
− 365	3.6
− 381	3.3
− 423	1.9
− 465	1.5
− 508	0.9
− 529	0.8
− 571	0.3

$x = 2$, $\alpha = 9°.69$, $\delta = 40°.64$

v	T
− 301	0.3
− 325	0.7
− 344	1.3
− 365	2.3
− 385	2.4
− 386	3.1
− 406	2.7
− 407	2.9
− 428	3.2
− 449	3.0
− 491	2.4
− 533	2.1
− 576	0.8
− 618	0.0

$x = 3$, $\alpha = 9°.49$, $\delta = 40°.45$

v	T
− 340	0.2
− 382	1.6
− 424	2.7
− 466	3.0
− 509	5.0
− 522	4.2
− 530	6.0
− 551	4.8
− 572	2.6
− 614	0.4
− 656	0.2

$x = 4$, $\alpha = 9°.28$, $\delta = 40°.25$

v	T
− 364	0.2
− 386	0.6
− 406	0.7
− 448	2.0
− 491	3.2
− 512	4.6
− 533	6.9
− 554	5.4
− 575	2.4
− 596	0.5
− 617	0.3

$x = 5$, $\alpha = 9°.08$, $\delta = 40°.05$

v	T
− 406	0.5
− 448	1.2
− 490	2.6
− 511	3.6
− 532	4.5
− 554	3.5
− 575	1.1
− 597	− 0.1

$x = 6$, $\alpha = 8°.89$, $\delta = 39°.86$

v	T
− 406	0.0
− 448	0.6
− 490	2.3
− 511	3.6
− 522	2.9
− 532	2.9
− 574	0.4

$x = 7$, $\alpha = 8°.69$, $\delta = 39°.66$

v	T
− 446	0.2
− 488	2.2
− 509	4.3
− 530	2.8
− 573	0.3
− 594	0.2

$x = 8$, $\alpha = 8°.50$, $\delta = 39°.46$

v	T
− 469	0.4
− 489	1.3
− 510	3.4
− 531	2.1
− 553	0.5

$x = 9$, $\alpha = 8°.30$, $\delta = 39°.26$

v	T
− 470	0.2
− 489	0.5
− 510	1.6
− 532	0.9
− 554	0.4

$x = 10$, $\alpha = 8°.11$, $\delta = 39°.07$

v	T
− 472	0.1
− 490	0.5
− 511	0.8
− 532	0.4
− 554	0.1

$x = 11$, $\alpha = 7°.92$, $\delta = 38°.87$

v	T
− 405	− 0.2
− 447	− 0.2
− 489	− 0.2
− 511	0.2
− 532	0.3
− 557	− 0.6

© Astronomical Institutes of The Netherlands • Provided by the NASA Astrophysics Data System

1957BAN....14..1V

The least-squares solution of u_1, by which $\Sigma p\Delta^2$ is minimized is

$$u_1 = -\frac{\Sigma ps\Delta'}{S_1} \pm \frac{\eta}{\sqrt{S_1}} \text{ (mean error)}.$$

Here $S_1 = \Sigma ps^2$ and all sums refer to the points of profile 1 only. The correction u_2 of profile 2 is found from the analogous formula with $S_2 = \Sigma ps^2$ for all points of profile 2. The final velocity of the centre then is

$$v_c = v_c' + \tfrac{1}{2}(u_1 + u_2) \pm \tfrac{1}{2}\eta\left(\frac{1}{S_1} + \frac{1}{S_2}\right)^{\frac{1}{2}}.$$

The mean errors in the first eight lines of Table 4 have been computed from this formula. Weights were assigned as following from the preceding section. The value $\eta = 0.25$°K was adopted throughout; this is more correct than to determine η from the residuals as the residuals tend to be kept low by changing the form of the curve. Some smoothness requirement must be imposed on the final curve in order to make the problem determinate. In the present method this condition is imposed by drawing the empirical curve through the points and by the assumption that s does not change by a small shift. Closely related problems have been discussed before by DE KORT (1941) and by KWEE and VAN WOERDEN (1956).

The weighted average of the independent determinations given in Table 4 is $v_c = -296 \pm 3$ km/sec. When the Mt Wilson and Lick measurements (HUMASON, MAYALL and SANDAGE, 1956) are also reduced to the local standard of rest by subtracting -4 km/sec, the values in the last two lines are obtained. They are given with estimated mean errors (Mt Wilson, authors' estimate converted from probable to mean error; Lick, our estimate).

A systematic difference between the results from points near the centre and those from more distant points is seen. A systematic position error of 0°.02 in the points at $x = 0, \pm 1$ would give a systematic error in v_c of about 10 km/sec. Such an error is unlikely but not impossible. The determination of v_c from more distant points is insensitive to this error. However, the rotational velocity may show real differences along the NE and SW axis. In view of these uncertainties we have adopted the weighted mean, -296 km/sec, as the true velocity of M31 with respect to the local standard of rest.

4. *Formulae for theoretical line profiles*

The main problem in the reduction is the enormous size of the antenna pattern relative to the details in the nebula that we might wish to distinguish.

If fully accurate line profiles at each point of the nebula were available, a logical reduction method would be to treat each frequency separately. The isophote map at each frequency might then be corrected for distortion by the antenna pattern and the corrected intensities might be combined into true line profiles at any point of the nebula. This scheme of reduction is partly followed in section 8 (p. 15).

The present data of limited accuracy, which are confined to the major axis, require additional assumptions in order to make the reduction feasible. The assumptions made in most of this paper are: circular symmetry and perfectly circular motion.

We assume that the hydrogen density in M31 is concentrated near one plane, so that for the present purpose its distribution may be characterized by the integrals

$$N = \int_{-\infty}^{\infty} n_{\mathrm{H}}\, dz, \qquad (5)$$

where n_{H} is the number of H atoms per cm^3 and z is the coordinate perpendicular to this plane. A point in the plane is represented by polar coordinates (a, φ), where a is the distance from the centre and $\varphi = 0$ on the major axis in the SW direction. We assume circular symmetry in each half of the nebula, so that the hydrogen distribution in the NE half and SW half may be described by separate functions $N(a)$.

The integral of the hydrogen density along the line of sight is $N(a)$ cosec i, where i is the angle between the plane of the nebula and the line of sight. We assume that cosec $i = 4$, so that the nebula is foreshortened in the ratio $\frac{1}{4}$. This value is within the range of values estimated from optical data (SCHMIDT, 1957b).

The motion will be assumed to be along perfectly circular orbits with the velocity $V(a)$ sec i. From here on we understand by v the velocity component in the line of sight relative to the centre of the nebula. In this notation, the abscissa of Figure 5 is $v_c + v$, where $v_c = -296$ km/sec and

$$v = -V(a) \sec i \,.\, \cos i \cos\varphi = -V(a)\cos\varphi. \qquad (6)$$

The minus sign arises from the fact that negative v (approach) occurs on the SW semi-axis, where we have put $\varphi = 0$.

The aim of the reduction is to find $N(a)$ and $V(a)$. If the antenna pattern would cover only a minute area on the nebula, these values could be read from the line profile obtained at a single point (a, φ). For, the width of the profile would arise from random cloud motions only, the profile would be centred at the velocity $-V(a)\cos\varphi$, and the integral of the profile would give $N(a)$ by

$$N(a) \text{ cosec } i = 6.0 \times 10^{-4} \int_{-\infty}^{\infty} T\, dv. \qquad (7)$$

Here T is brightness temperature in the line in °K,

© Astronomical Institutes of The Netherlands • Provided by the NASA Astrophysics Data System

1957BAN....14....1V

v is measured in km/sec, and $N(a)$ is expressed in cm^{-3} kpc.

Equation 7 excludes the effect of selfabsorption, which will later be shown to be small. If c.g.s. units are employed the constant in eq. 7 is

$$\frac{32\pi k}{3Ahc\lambda^2} = 1.84 \times 10^{13},$$

where k = Boltzmann's constant, h = Planck's constant, c = velocity of light, A = transition probability and $\lambda = 21.10$ cm. A derivation is found in *B.A.N.* No. 452, eq. 12 (VAN DE HULST, MULLER and OORT, 1954). The constant given here follows by a conversion of cm into kpc and of cm/sec into km/sec.

The antenna pattern is assumed to be perfectly circular. The antenna sensitivity at the distance r from the centre of the pattern is a known function $p(r)$ (Table 1). We write

$$\int_0^\infty 2\pi r p(r)\, dr = P. \qquad (8)$$

The units of a and r are arbitrary; in the computation we choose 1 unit = 0°.25. In these units, $P = 5.50$.

FIGURE 6

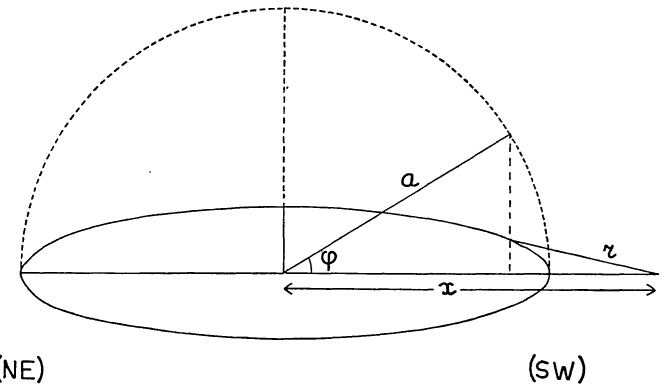

Geometrical quantities.

Let the antenna be centred on a point of the major axis, at $a = x$, $\varphi = 0$. The r for an arbitrary point (a, φ) then is given by (Figure 6)

$$r^2 = (x - a\cos\varphi)^2 + (\tfrac{1}{4} a \sin\varphi)^2, \qquad (9)$$

where we have substituted $\sin i = \frac{1}{4}$. For fixed x and a, r reaches a minimum or maximum at $\varphi = 0$, a maximum at $\varphi = 180°$, and a minimum at $\cos\varphi = 16x/15a$ if this is < 1. In the latter minimum the circle with radius r is tangent at the inside to the ellipse with semi-major axis a and $r^2 = a^2/16 - x^2/15$.

Writing eq. 7 for each point within the antenna pattern, multiplying by $p(r)/P$ and integrating over the sky we obtain at both sides the weighted average with $p(r)$ as a weighting factor:

$$\frac{1}{P}\int_0^\infty\int_0^{2\pi} N(a)p(r)\,a\,da\,d\varphi = 6.0 \times 10^{-4}\int_{-\infty}^{\infty} Tdv. \qquad (10)$$

At the left-hand side, r is a function of x, a and φ, by eq. 9; the foreshortening factor $\frac{1}{4}$ cancels the factor 4 by which the path through the nebula exceeds the perpendicular path. At the right-hand side, $T(v)$ now denotes the observable intensity in the line profile. We shall denote the right-hand side by 4 $J(x)$; the function

$$J(x) = 1.5 \times 10^{-4}\int_{-\infty}^{\infty} Tdv \qquad (11)$$

may be obtained at once from the measured line profiles by integration. The definition implies that $J(x) = N$ if the antenna pattern would be filled by a part of the nebula with virtually constant N.

Equation 10 is an integral equation from which $N(a)$ has to be solved. Performing the integration over φ transforms eq. 10 into

$$\int_0^\infty N(a) f_x(a)\, da = J(x), \qquad (12)$$

where

$$f_x(a) = \frac{a}{2P}\int_0^\pi p(r)\, d\varphi\,. \qquad (13)$$

The functions $f_x(a)$ were computed by graphical integration from eqs. 13, 9, and Table 1. The relation

$$\int_0^\infty f_x(a)\, da = 1 \qquad (14)$$

for each x, which follows from the definition, served as a check on the computations. Graphs of $f_x(a)$ are presented in Figure 7.

FIGURE 7

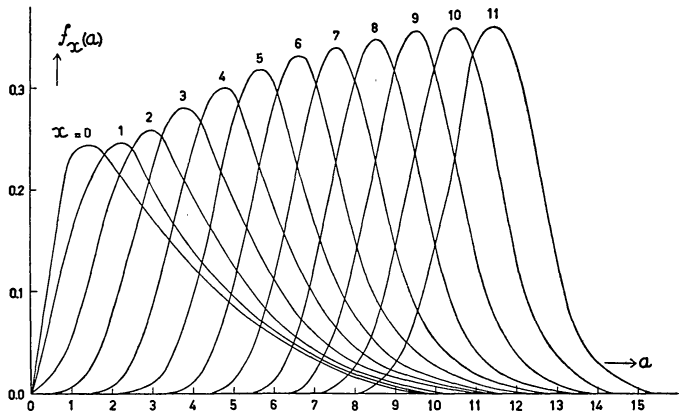

Functions showing the weights by which matter at a distance a from the centre of the nebula enters into an observation at point x.

Additional functions are required for computing the line profiles. Besides the integrals (11) and (13) we introduce the incomplete integrals:

$$J(x, v_1) = 1.5 \times 10^{-4}\int_{-\infty}^{v_1} Tdv \qquad (15)$$

so that $J(x, -\infty) = 0$, $J(x, \infty) = J(x)$.

© Astronomical Institutes of The Netherlands • Provided by the NASA Astrophysics Data System

1957BAN....14..1V

And, likewise,

$$f_x(a, \varphi_1) = \frac{a}{2P}\int_0^{\varphi_1} p(r)\, d\varphi \qquad (16)$$

so that

$$f_x(a, 0) = 0, \quad f_x(a, \pi) = f_x(a).$$

Clearly, $J(x, v_1)$ is the part of $J(x)$ that corresponds to velocities $< v_1$ and $f_x(a, \varphi_1)$ is the part of $f_x(a)$ that corresponds to $\varphi < \varphi_1$. Hence we may write at once

$$\int_0^\infty N(a) f_x(a, \varphi_1)\, da = J(x, v), \qquad (17)$$

where

$$\left.\begin{aligned} \varphi_1 &= 0 && \text{for } v \leqq -V(a) \\ \cos\varphi_1 &= -v/V(a) && \text{for } |v| < V(a) \\ \varphi_1 &= \pi && \text{for } v \geqq V(a) \end{aligned}\right\} \qquad (18)$$

The function φ_1 of v and a defined by (18) will be denoted by $\varphi(v, a)$.

Random cloud motions and instrumental band width have not yet been considered in this derivation. The line profile without these broadening effects would be given by

$$1.5 \times 10^{-4}\, T(x, v) = dJ(x, v)/dv. \qquad (19)$$

The broadening effects can easily be taken into account if they have a rectangular distribution, i.e., if they spread a peak at velocity v evenly over the range of velocities from $v - \frac{1}{2}\Delta v$ to $v + \frac{1}{2}\Delta v$. The line profile then is given by

$$1.5 \times 10^{-4}\, T(x, v) = \frac{J(x, v + \frac{1}{2}\Delta v) - J(x, v - \frac{1}{2}\Delta v)}{\Delta v}. \qquad (20)$$

Other distribution functions might be taken into account by a folding integral, but this refinement is not needed.

The method for computing a line profile outlined here has a practical advantage over a method in which the amount of radiation in the velocity interval dv would be computed directly. The singularities in the integrands which would occur in the points where $dv/d\varphi = 0$, are avoided in the present method.

5. *Density distribution*

The integrals of the line profiles, $J(x)$, obtained from Figure 5, have been plotted as a function of x in Figure 8. The numbers may be read from Table 5 by summing the two halves. If the density distribution would have circular symmetry in the entire nebula, Figure 8 would be symmetric and $N(a)$ could be found by solving eq. 12. As Figure 8 is not quite symmetric, we reduced each half of the nebula separately. Positive v occurs only in the NE half and negative v only in the SW half, if we assume perfectly circular motion with an arbitrary rotation law $V(a)$.

FIGURE 8

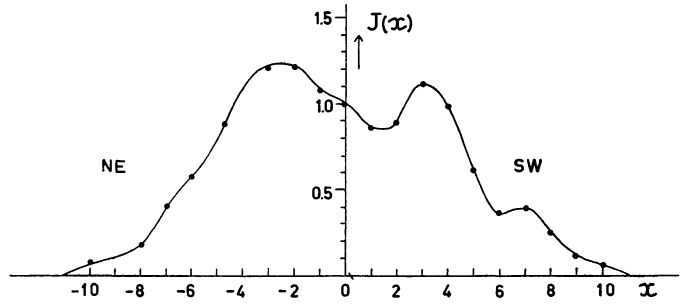

Integrals of observed line profiles

The corrections caused by random cloud velocities of the usual order are negligible. We write

Emission by SW half: $J'(x) = J(x, 0)$
$f'_x(a) = f_x(a, \pi/2)$

Emission by NE half: $J''(x) = J(x) - J(x, 0)$
$f''_x(a) = f_x(a) - f_x(a, \pi/2)$.

The relation replacing eq. 12 for the SW half of the nebula then is

$$\int_0^\infty N(a) f'_x(a)\, da = J'(x) \qquad (21)$$

and similarly for the NE half. The values of $J''(x)$ and $J'(x)$ found by measuring the areas of the profiles in Figure 5 left and right of the centre velocity are given in Table 5 and in Figure 9.

FIGURE 9

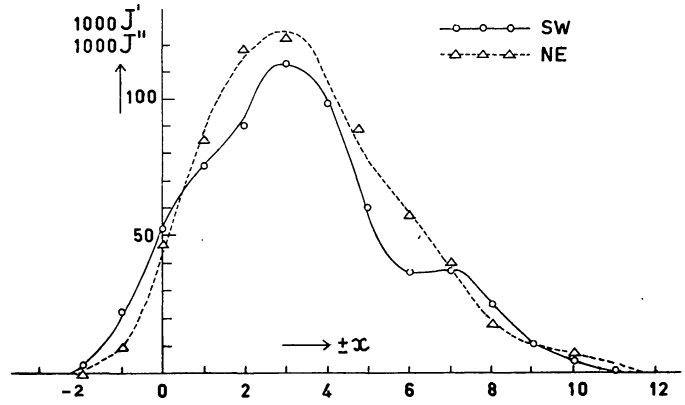

Integrals of observed line profiles for positive and negative velocities. Circles and triangles: observations. Solid and dotted curves: computations.

For a convenient solution, we define the average values of $N(a)$ in successive elliptical rings by

$$\begin{aligned} q_0 &= 8\int_0^{\frac{1}{2}} N(a)\, a\, da \\ q_a &= \frac{1}{a}\int_{a-\frac{1}{2}}^{a+\frac{1}{2}} N(a)\, a\, da, \quad a = 1, 2, 3, \ldots \end{aligned} \qquad (22)$$

Next, we consider the hydrogen of each ring concen-

© Astronomical Institutes of The Netherlands • Provided by the NASA Astrophysics Data System

1957BAN....14....1V

trated in sharp rings at $a = 1, 2, 3, \ldots$ and a dot at $a = 0$. Equation 21 then becomes the set of linear equations

$$J'(x) = \frac{\pi}{32P} q_0 p(|x|) + \sum_{a=1}^{\infty} q_a f'_x(a). \quad (23)$$

The solution for q_a can be made with fair precision by starting at large a and applying subsequent corrections to minimize the residuals. The values of q_a that were found to give the best solution are given in Table 6. The corresponding values of $J'(x)$ are entered as "computed" in Table 5 and are represented by the curves in Figure 9. The residuals are small.

Minor changes in the coefficients do not greatly impair the agreement. For instance, if at the SW side the top numbers are replaced by $q_0 = 50$, $q_1 = 11$, the residuals (obs. — comp.) rise to $+7$ at $x = -1$ and -5 at $x = 2$. This modified solution is shown in the graph of the density distribution in Figure 10. The averages of $q_a = \overline{N}(a)$ obtained for the SW and NE halves are represented by the step curve of Figure 10.

FIGURE 10

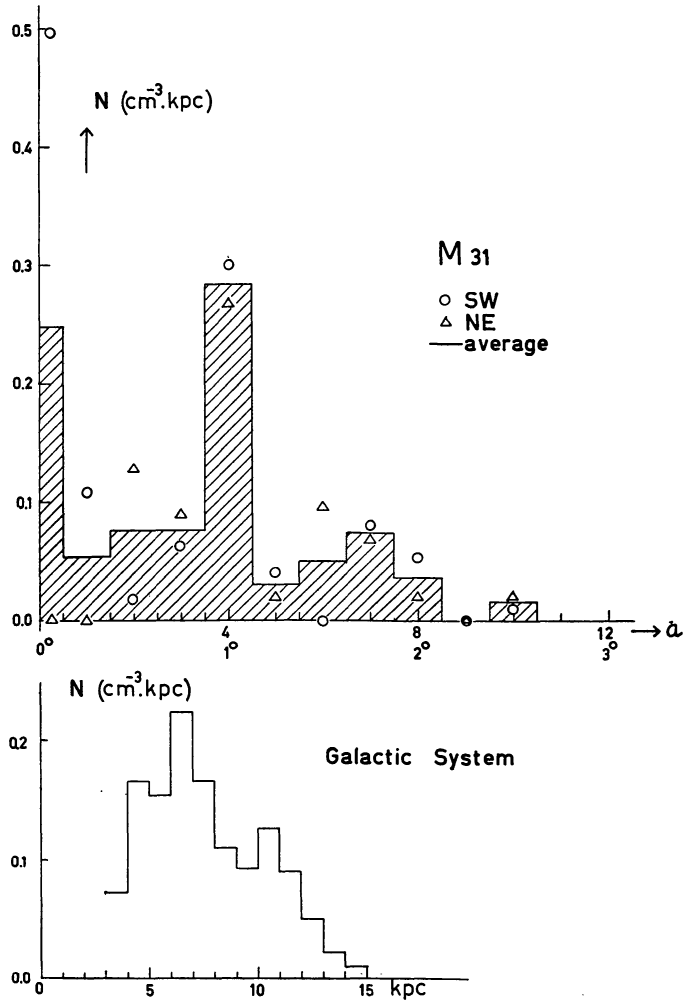

Density distribution in M31 and in the Galactic System.

TABLE 5

Integrals of line profiles

Emission by SW half				Emission by NE half				„Model"
x ($\frac{1}{4}°$)	1000 J' obs.	comp.	diff.	x ($\frac{1}{4}°$)	1000 J'' obs.	comp.	diff.	
− 2	3	2	1	2	0	1	− 1	1
− 1	23	19	4	1	10	10	0	16
0	53	53	0	0	47	44	3	48
1	76	76	0	− 1	85	88	− 3	82
2	90	93	− 3	− 2	118	115	3	103
3	113	113	0	− 3	122	125	− 3	118
4	98	99	− 1	− 4		106		103
5	61	57	4	− 5	89*	77	4*	65
6	37	37	0	− 6	58	59	− 1	50
7	38	38	0	− 7	41	40	1	40
8	25	26	− 1	− 8	18	19	− 1	22
9	11	11	0	− 9		10		10
10	5	5	0	− 10	8	7	1	6
11	1	1	0	− 11		3		2

* These values refer to $x = -4.7$

TABLE 6

Density distribution

a ($\frac{1}{4}°$)	100 q_a = 100 $\overline{N}(a)$ SW	NE	"Model"
0	100 (50)	0	38
1	5 (11)	0	5
2	2	13	7
3	6	9	7.5
4	30	27	28.5
5	4	2	3
6	0	10	5
7	8	7	7.5
8	5	2	3.5
9	0	0	0
10	1	2	1.5

TABLE 7

Rotation law

a ($\frac{1}{4}°$)	$V(a)$ "Model"	V_{rot} final value
0	0 km/sec	0 km/sec
$\frac{1}{2}$	100	103
1	187	193
$1\frac{1}{2}$	234	241
2	259	267
$2\frac{1}{2}$	270	278
3	267	275
4	255	263
5	243	249
6	236	242
7	230	235
8	226	231
9	221	226
10	216	221

© Astronomical Institutes of The Netherlands • Provided by the NASA Astrophysics Data System

1957AN....14....1V

6. *Rotation law and line profiles*

The sharp line profiles observed at $|x| \geqq 4$ permit a precise determination of the rotation curve $V(a)$ in the outer parts of the nebula, $a \geqq 4$. At a first glance we see from the position of the maxima that $V(a)$ is of the order of 200 to 250 km/sec throughout this region and that it does not strongly decrease with increasing distance from the centre. A more precise determination requires a calculation of model line profiles which takes the radiation from all areas inside the antenna beam into account.

After some preliminary tries, we adopted the following specification for the computation of the line profiles.

Density distribution: Column "Model" in Table 6. This is about the average of the values found for the two halves; it did not seem necessary at this stage to double the labour by separate computations for the two halves, although this would undoubtedly have improved the agreement with observation.

Rotation curve: Column "Model" in Table 7.

Line broadening: The effects of random cloud velocities and of instrumental bandwidth combined were taken into account by taking the average value of $T(v)$ over intervals $\Delta v = 60$ km/sec.

The line profiles for this model were computed by means of eqs. 16, 17, 18 and 20 for $x = 0, 1, \ldots 11$ at intervals of 20 km/sec in v. They are represented by the dotted curves in Figure 5. The integrals $J'(x)$ served as a check on the computation. As shown in Table 5, they are very nearly the average of the values observed for the two halves.

The model profiles represent the observed ones quite well, especially if we consider that only two functions, $N(a)$ and $V(a)$, were left to choice. The density distribution is based exclusively on the *areas* under the profiles. The rotation law has been chosen to give the profiles for $|x| \geqq 4$ the correct *position*; for $a \leqq 3$ it is essentially a guess made after the example of the rotation law in the Galactic System (see Figure 11). The *shape* and *width* of the profiles were fixed by these data, and do not depend on any further choice, except for a minor broadening effect by random cloud velocities. Striking points of agreement between observations and model are: the shape of the central profile ($x = 0$) with its wide wings of low intensity; the peculiar change of shape from $x = 0$ to $|x| = 3$ by which at $|x| = 2$ a profile without a clear-cut maximum results; and the asymmetry in the profiles from $|x| = 4$ to $|x| = 6$.

A number of corrections and refinements may now be considered.

Rotation curve ($a \geqq 4$). A shift of $V(a)$ will shift the corresponding line profiles by about the same amount. Inspection of Figure 5 shows that 5 km/sec is about the maximum shift that is permissible on the SW axis (positive x); possibly, $V(a)$ would have to be lowered by 2 km/sec. The data on the NE axis are less reliable because of the galactic foreground. At $x = -6$, -7, and -8, the values of $V(a)$ indicated by the observations seem to be about 10 km/sec higher than those adopted in the model but the uncertainty is of the same order. The final rotation velocities V_{rot} for $a \geqq 4$ given in Table 7 have been found from the model by subtracting 1 or 2 km/sec and adding 3% for the inclination effect.

FIGURE 11

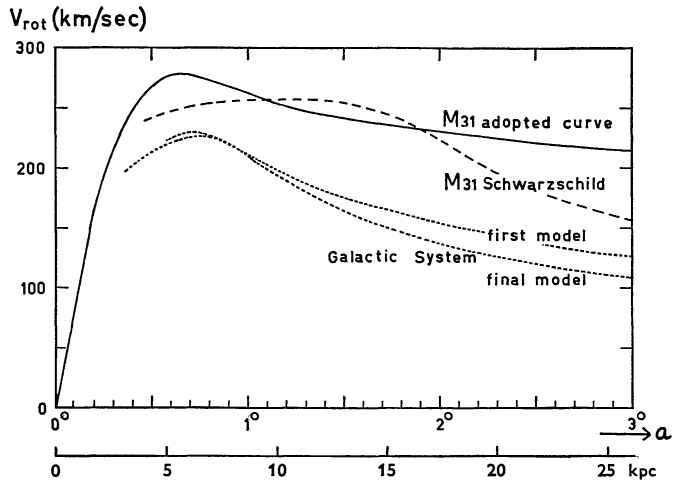

Rotation laws of M31 and the Galactic System.

FIGURE 12

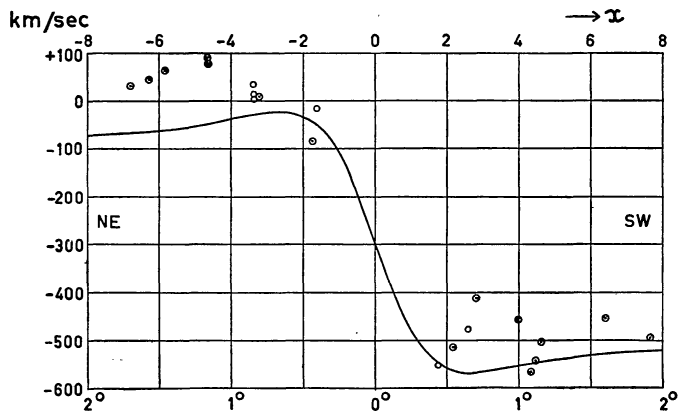

Radial velocities in points of the major axis of M31 with respect to the local standard of rest. Full curve: based on radio data. Circles : optical data.

The optical data, though less accurate, may be shown for comparison. In Figure 12 we have plotted the radial velocity with respect to the local standard of rest in points of the major axis. The full-drawn curve represents the velocity $-296 \pm V(a)$ derived from the radio data. The circles represent emission nebulae whose velocities have been measured by

© Astronomical Institutes of The Netherlands • Provided by the NASA Astrophysics Data System

1957BAN....14....1V

MAYALL (1950). They have been reduced to the major axis by a correction $\pm\left(1-\frac{x}{a}\right)V(a)$, where $a=\sqrt{x^2+(4y)^2}$ and $V(a)$ is taken from Table 7. Circles with dots represent points for which this correction is <30 km/sec (average: 8 km/sec) and small circles represent points with corrections >30 km/sec (average: 104 km/sec). Points weighted $\frac{1}{2}$ or 1 in MAYALL's list have been omitted. A further correction of + 4 km/sec has been applied to refer all velocities to the local standard of rest. The agreement between optical and radio data in Figure 12 is rather poor and the systematic deviation of nearly 100 km/sec in the NE half is disconcerting.

Selfabsorption; density at $a=4$. The fact that the maximum brightness temperature in the line profiles is only 8°K does not prove the absence of selfabsorption, for the beamwidth and bandwidth cause only an apparent widening of the line. The actual line at a projected point of the nebula is widened by the spread in velocities along the line of sight, which arises from two effects. *a*. Systematic variations along the line of sight. The line of sight cuts the planes $z=+125$ pc and $z=-125$ pc at points which are 1 kpc apart in the projection on the plane of the nebula. This effect by itself gives a line width of 10 to 60 km/sec at points outside the major axis but virtually zero width on the major axis. *b*. Random cloud velocities with root mean square value in one component, $\sigma=8$ km/sec (see below) give a line width between half-power points of 19 km/sec.

Adopting for a moment a rectangular line profile with width 20 km/sec, we find by eq. 7 that the true brightness temperature within the line at any point of the model nebula is

$$T_m=\frac{N(a)}{0.0030}.$$

By Table 6 the peak is $T_m=95$°K at $a=4$. As this is not small compared with the gas temperature, a correction for selfabsorption is required. In all other rings T_m remains below 25°K and selfabsorption may be neglected. The value $T_m=127°$ at $a=0$ refers to a minute area in which the density is very uncertain.

For a quantitative estimate of the density correction, we assume that the ring of high density at $a=4$ is exactly 1 unit wide, as drawn in Figure 10. It might actually be wider or narrower, or it might be patchy. Further we assume the hydrogen temperature $T_0=125°$ and a gaussian velocity distribution with $\sigma=10$ km/sec as the combined effect of *a* and *b*, above. The theory of selfabsorption of a line with pure Doppler broadening (e.g., UNSÖLD, 1938, p. 168) then gives a ratio 0.75 between the area of the line affected by selfabsorption and the area unaffected by selfabsorption. Consequently, the density in the ring may be put $N(a)=0.285/0.75=0.38$.

Under the very schematic assumption that σ is the same in all points of the elliptical ring, the computation of the model profiles in Figure 5 remains correct if we take selfabsorption into account and use the higher value of $N(a)$. Actually, effect *a* differs in various points of the ring; this complicates the situation and probably reduces the overall correction needed.

It may be noted that a further uncertainty in the determination of the hydrogen density both in M31 and the Galactic System lies in the assumption that individual clouds are optically thin. The optical depths of the order of 3 found by MULLER (1957) for the clouds in front of the Cassiopeia source throw some doubt on this assumption. A further increase in the calculated hydrogen density in both systems may therefore be needed.

Densities at $a>4$. The values given in Table 6 for each half separately are certainly better than the average values used in the model. Further corrections are not needed.

Random cloud velocities. The dotted curves in Figure 5 show that the choice of a rectangular profile with $\Delta v=60$ km/sec represents a good approximation to the combined broadening effect by bandwidth and random cloud velocities. In an earlier calculation $\Delta v=30$ km/sec was used. Addition of 0.3 times the second difference of the numbers tabulated at intervals of 20 km/sec then proved necessary in order to obtain agreement with the observations.

To interpret these results, it is sufficient to consider only the r.m.s. velocity deviation σ (in km/sec) of each broadening function. The σ^2 of the cloud velocities may then be found by subtracting the instrumental σ^2 from the σ^2 fitting the observations. Suppressing the details of the calculation we have

		σ	σ^2
a. rectangular band, $\Delta v=60$		17.3	300
b. rectangular band, $\Delta v=30$		8.7	75
0.3 × second difference		15.5	240
together		17.7	315
c. instrumental bandwidth		15.4	239
difference due to cloud motion	$a-c$	7.8	61
	$b-c$	8.7	76

The small difference left for the cloud velocities is evidently uncertain. Yet it is gratifying to see that both estimates lead to r.m.s. velocity components in the line of sight of the order of 8 km/sec. The actual value might range from 5 to 10 km/sec and is of the same order as found in the Galactic System.

© Astronomical Institutes of The Netherlands • Provided by the NASA Astrophysics Data System

1957AN....14...1V

Densities and rotation law at $a \leqq 3$. The situation in the inner part is less clear than in the outer regions of the nebula. The densities obtained from the integrals (Table 6) should be about correct, with the understanding that the separation into two halves and into discrete rings should not be taken literally. These results have the advantage of being largely independent of any assumption about the motions. The rotation curve is far less reliable; the only conclusion that can be drawn from Figure 5 is that a curve of this general character represents the data satisfactorily.

Some of the differences between observed and computed profiles, e.g. the bulge at − 220 km/sec, $x = -2$ and -3, do not occur at the other side of the centre. They may be local deviations that require further study (see also sec. 8). Other differences, e.g., at $x = \pm 2$ from 160 to 240 km/sec from the centre, are symmetric. They might be remedied by minor adjustments in the density distribution and/or rotation law.

7. *Comparison with the Galactic System*

The Andromeda nebula (M31) and the Galactic System are both classed as Sb spirals. The data published in the literature do not indicate any obvious differences between the two systems.

The distance of M31 is still uncertain. We shall adopt a distance of 500 c kpc. Here c is a possible correction factor that will be taken into all formulae. At present we take $c \approx 1$ as the likeliest estimate. It is perfectly well possible, however, that $c = 1.26$, $r = 630$ kpc (SCHMIDT, 1957b) may turn out to be better. The unit of a in the previous sections is

$$\tfrac{1}{4}^\circ = 2.18\ c \text{ kpc}.$$

The density distributions of atomic hydrogen in M31 (Table 6) and the Galactic System (WESTERHOUT, 1957) are compared in Figure 10. The scale of abscissae is equal if $c = 1$. The scale of ordinates is based on the assumption that in the Galactic System $N = \bar{n}_H$ (cm^{-3}) × 0.22 (kpc) (SCHMIDT, 1957 a). Both figures give the average densities over fairly wide rings so that a detailed correspondence of maxima with spiral arms cannot be expected. BAADE (1956) mentions the existence of 7 spiral arms along the SW axis within 2° from the centre ($x = 0$ to 8), in which range Figure 10 shows only two maxima.

The high-density ring at $x = 4$ ($= 8.7\ c$ kpc) in the distribution derived for M31 is undoubtedly real. The deficiency of hydrogen in the inner parts of the system is also apparent from the dip in Figure 8. The other peak in Figure 10, at the centre of M31, is much less certain. The hydrogen distribution in the Galactic System seems to show a similar ring at somewhat smaller distance from the centre. The difference between the radii of the rings in both systems becomes more pronounced if $c = 1.26$.

A striking difference in the two distributions in Figure 10 is that the hydrogen in the Galactic System extends to a smaller distance and decreases more abruptly than in M31. The presence of a tail, as seen in the upper figure up to $x = 10$ (22 c kpc), could not have escaped notice in the galactic studies made at Kootwijk (WESTERHOUT, 1957), unless it would have a very wide z-distribution. The hydrogen densities in M31 decrease roughly in proportion to the light; both are measurable to distances of nearly 3° from the centre. The light, in turn, is roughly proportional to the total mass density (SCHMIDT, 1957 b). A similar comparison for the Galactic System is not well possible as the rotation curve in the outer parts and, therefore, the distribution of mass is not known from observations.

The total amount of atomic hydrogen in M31 is

$$M_H = m_H \int_0^\infty N(a)\ 2\pi a\ da,$$

where m_H is the mass of the hydrogen atom. Table 6 gives

$$\int_0^\infty N(a)\ a\ da = \tfrac{1}{8}\ q_0 + \sum_{a=1}^{\infty} a\ q_a = 3.01 \text{ cm}^{-3} \text{ kpc } (\tfrac{1}{4}^\circ)^2.$$

By the correction for selfabsorption in the ring $a = 4$ this is increased to 3.39. We thus find

$$M_H/m_H = 2\pi \times (2.18\ c)^2 \times 3.39 = 101\ c^2 \text{ cm}^{-3} \text{ kpc}^3$$

and upon multiplication by $(m_H/M_\odot)$ (1 kpc/1 cm)^3 $= 2.5 \times 10^7$ we obtain

$$M_H = 0.25 \times 10^{10}\ c^2\ M_\odot .$$

This may at once be compared with the total mass of M31 found by SCHMIDT (1957b) for a model mass distribution that fits the rotation curve in Figure 11. This mass is

$$M = 26.8 \times 10^{10}\ c\ M_\odot ;$$

it is 1.8 times the result of SCHWARZSCHILD (1954). The ratio is $M_H/M = 0.01\ c$; the atomic hydrogen thus forms 1, or possibly 1.3, per cent of the mass of M31.

The hydrogen density in the Galactic System may be integrated in a similar manner and gives

$$M_H/m_H = 2\pi \times 0.22 \times 44 = 61 \text{ cm}^{-3} \text{ kpc}^3$$

and hence

$$M_H = 0.15 \times 10^{10}\ M_\odot ,$$

whereas the total mass in the "final model" computed by SCHMIDT (1956) is

$$M = 7.0 \times 10^{10}\ M_\odot .$$

© Astronomical Institutes of The Netherlands • Provided by the NASA Astrophysics Data System

1957BAN....14....1V

This mass is less certain than the mass of M31 because the rotation law in the Galactic System at distances well beyond the sun is not known from observation. In view of the observations on M31 it might be conjectured that the rotational velocity falls less sharply with increasing distance from the centre than has been assumed. This would lead to a higher mass, e.g., the value 10×10^{10} $M_\odot$ found in SCHMIDT's first model. It may be concluded that atomic hydrogen forms 1 to 2 per cent of the total mass of the Galactic System.

The total mass of M31 is 3 to 4 times that of the Galactic System; the atomic hydrogen mass in M31 is 2 times that in the Galactic System.

8. *Observations at one velocity*

A special programme, carried out during the last days of the observing period, was devoted to observations at one velocity, $v = -224$ km/sec with respect to the local standard of rest, i.e. $+72$ km/sec with respect to the centre of M31. Unlike the observations collected in Figure 5, this programme included points outside the main axis of the nebula. The antenna temperatures observed at this velocity are shown in Table 8. Negative x is measured along the major axis in the NE direction, as before, and y is measured along the minor axis in the NW direction; the unit in both coordinates is $\frac{1}{4}°$. For the fields with $y = 0, -1$, and -2, the method of observation differed from that described in sec. 1, in that a continuous sequence of 15-minute measurements was made in which the standard field ($x = -2$, $y = 0$) occurred 9 times, each of the other fields twice, and the comparison field ($\alpha = 15°.00$, $\delta = 41°.00$) only once.

Full observations of this type, when repeated at many velocities, might serve for a solution of the density and motions in the system without any symmetry assumptions. This programme had a more direct aim. The steepness of the rotation curve in the central parts of the system can be determined, in principle, by finding the point on the major axis at which a certain velocity is reached. The velocity of $+70$ km/sec was chosen. According to the "model" curve of Figure 11, this is reached at $x = -0.4$. The finite size of the antenna beam shifts this point away from the centre. For instance, the ring of heavy density at $a = 4$ gives rise to this velocity, according to the model, in the points $x = -1.10$, $y = \pm 0.96$. The expectation, therefore, was that in scanning with the centre of the beam along the major axis the maximum temperature would be reached somewhere between $x = -0.4$ and -1.1. The fact that the observations seemed to contradict this expectation suggested the special programme now under discussion.

TABLE 8

	$x = -3$	-2	-1	0
$y = 2$		1.8	2.0	
$y = 1$		3.3	3.4	
$y = 0$	1.8	3.4	4.1	1.8
$y = -1$	1.8	2.9	2.8	1.0
$y = -2$	0.6	1.1	0.7	0.1
From Figure 5, $y = 0$	(1.9)	(4.0)	(3.2)	(1.2)

A theoretical computation with the full antenna pattern taken into account gave indeed a maximum at $x = -1.0$. However, in interpolating between the data of Figure 5, the maximum was found

for $v = +70$ km/sec at $x = -1.8$
for $v = 0$ km/sec at $x = -0.1$
for $v = -70$ km/sec at $x = +1.1$

The accuracy is about 0.1 unit in x, or poorer if systematic changes in sensitivity from day to day have occurred. The measurements of the special programme (Table 8) are free from such errors. They give a maximum

for $v = +72$ km/sec at $x = -1.4 \pm 0.1$.

The difference with the computed value $x = -1.0$ probably is significant but no good explanation has been found. The following possibilities were checked.

a) BABCOCK (1939) has measured a rotation curve with a dip in the central parts of the nebula. Later, the suspicion arose that the dip might have been caused by stray light. Let us assume, in accordance with these data, that v goes up to 100 at $x = \frac{1}{4}$, down to 0 again at $x = \frac{1}{2}$, and then up until it joins the "model" curve at $x = 3$. The value $v = +70$ km/sec then is reached for a narrow pencil beam at $-x = 0.12$, 0.33 and 1.05. But a computation with the actual antenna pattern gives one maximum at $x = -1.1$. Evidently, the change in the assumptions is not drastic enough to remove the discrepancy noted above. The motions inferred by LINDBLAD (1956) from his interpretation of M31 as a barred spiral deviate even less from regular rotation.

b) VAN WOERDEN, ROUGOOR and OORT (1957) have observed expansion in the central parts of the Galactic System. The obvious effect of a similar phenomenon in M31 would be an asymmetry between corresponding points of positive and negative y in Table 8. A sample computation indicated that the difference would be in the sense as shown in Table 8 but would not exceed 0.2°K. It should be noted that the data now available are not suitable for a precise check on expansion as the method of observation and reduction happened to be different for positive and negative y.

c) The fact that a similar discrepancy does not exist at the SW side ($v = -70$ km/sec) suggests a local density deviation. The locus of the points where

© Astronomical Institutes of The Netherlands • Provided by the NASA Astrophysics Data System

1957BAN....14....1V

$v = +70$ km/sec in the model passes through the points $x = -1.45, y = \pm 1.20$ ($a = 5$). An agglomeration of hydrogen near one of these points, or even farther away from the centre, would push the maximum on the main axis towards the observed position. The observations collected in Table 8 were made in the hope that it might be possible to confirm the existence of such an agglomeration directly. However, the results do not support this explanation. Model computations performed for all points in Table 8 gave the residuals (observed — computed) in Table 9. The theoretical values are based on a

TABLE 9

	$x = -3$	-2	-1	0
$y = \pm 2$	-0.4	-0.3	-0.1	-0.5
$y = \pm 1$	$+0.9$	$+1.0$	$+0.5$	-0.4
$y = 0$	$+1.0$	$+1.6$	$+0.9$	-0.3

model with a density distribution slightly different from Table 6. The observed values have been averaged for positive and negative y.

Table 9 suggests that the excess radiation at this frequency comes from a point on the main axis near $x = -2$. Material at this point partaking in the normal rotation in the plane of the nebula has the velocity 280 km/sec! It is very puzzling how radiation at the much lower velocity of $+70$ km/sec can be emitted from this point at all. More complete measurements at this and other frequencies are urgently needed.

Acknowledgements

An investigation of this type is so much a cooperative effort that it is hard to give proper acknowledgement to all persons whose help or labour has been essential for the successful completion of the programme. It may be emphasized, however, that observations of high quality were made possible not only by the availability of a big telescope but quite as much by the excellent performance of the receiver. This highly sensitive receiver was designed by C. A. MULLER and was built and kept in fine operating condition by him together with A. C. HIN.

The coordinate converter and accompanying servo system was designed by B. G. HOOGHOUDT, received maintenance from R. H. J. VAN 'T LAND, and was calibrated by means of astronomical observations by G. WESTERHOUT.

Considerable assistance in the observations was given by S. L. T. J. VAN AGT and W. J. VAN REEUWIJK. Certain parts of the numerical reduction were carried out by Miss L. M. J. S. VOLDERS and by S. LAUSTSEN. Dr M. SCHMIDT made the results of his calculations on the mass available before publication.

This work was made possible by the financial assistance from the Netherlands Organization for Pure Research (Z.W.O.).

REFERENCES

W. BAADE, 1956, "Mitt. Astr. Gesellschaft 1955", p. 51, Hamburg.
H. W. BABCOCK, 1939, *Lick Obs. Bull.* **19**, 41 (No. 498, Plate III).
H. C. VAN DE HULST, C. A. MULLER and J. H. OORT, 1954, *B.A.N.* **12**, 117 (No. 452).
H. C. VAN DE HULST, 1957, "Radio Astronomy", I.A.U. Symp. No. 4, Cambridge University Press, p. 3.
H. C. VAN DE HULST, B. G. HOOGHOUDT, R. J. SCHOR, W. HUISMAN, B. B. SCHIERBEEK, G. H. JÖBSIS, 1957, *De Ingenieur*, **69**, O.1
M. L. HUMASON, N. U. MAYALL and A. R. SANDAGE, 1956, *A.J.* **61**, 97.
J. DE KORT, 1941, *B.A.N.* **9**, 252 (No. 345).
K. K. KWEE and H. VAN WOERDEN, 1956, *B.A.N.* **12**, 327 (No. 464).
B. LINDBLAD, 1956, *Stockholm Obs. Ann.* **19**, No. 2.
D. A. MACRAE and G. WESTERHOUT, 1956, "Table for the reduction of velocities to the local standard of rest", Lund Observatory.
P. A. MANN and P. MEZGER, 1956, *Telefunken Zeitung* **29**, 182.
N. U. MAYALL, 1950, *Publ. Obs. Univ. Michigan*, **10**, 19.
C. A. MULLER, 1956, *Philips Techn. Rev.* **17**, 351.
C. A. MULLER, 1957, *Ap.J.* **125**, 830.
C. A. MULLER and G. WESTERHOUT, 1957, *B.A.N.* **13**, 151 (No. 475).
M. SCHMIDT, 1956, *B.A.N.* **13**, 15 (No. 468).
M. SCHMIDT, 1957a, *B.A.N.* **13**, 247 (No. 475).
M. SCHMIDT, 1957b, *B.A.N.* **14**, 17 (No. 480).
M. SCHWARZSCHILD, 1954, *A.J* **59**, 273.
A. UNSÖLD, 1938, "Physik der Sternatmosphären", Berlin, Springer.
G. WESTERHOUT, 1957, *B.A.N.* **13**, 201 (No. 475).
H. VAN WOERDEN, G. W. ROUGOOR and J. H. OORT, 1957, *Comptes Rendus* (Paris) **244**, 1691.

© Astronomical Institutes of The Netherlands • Provided by the NASA Astrophysics Data System